SAND2021-7613C

GRC Transactions, Vol. XX, 2021

# Analysis and Optimization of a Closed Loop Geothermal System in Hot Rock Reservoirs

**Yaroslav V. Vasyliv, Gabriela A. Bran-Anleu, Alec Kucala, Sam Subia, Mario J. Martinez**

**Sandia National Laboratories, Albuquerque, NM**

**Keywords**

*closed-loop systems, u-tube, parametric, optimization, FORGE site, hot dry rock*

## ABSTRACT

Recent advances in drilling technology, especially horizontal drilling, have prompted a renewed interest in the use of closed loop geothermal energy extraction systems. Deeply placed closed loops in hot wet or dry rock reservoirs offer the potential to exploit the vast thermal energy in the subsurface. To better understand the potential and limitations for recovering thermal and mechanical energy from closed-loop geothermal systems (CLGS), a collaborative study is underway to investigate an array of system configurations, working fluids, geothermal reservoir characteristics, operational periods, and heat transfer enhancements (Parisi et al., 2021; White et al., 2021). This paper presents numerical results for the heat exchange between a closed loop system (single U-tube) circulating water as the working fluid in a hot rock reservoir. The characteristics of the reservoir are based on the Frontier Observatory for Research in Geothermal Energy (FORGE) site, near Milford Utah. To determine optimal system configurations, a mechanical (electrical) objective function is defined for a bounded optimization study over a specified design space. The objective function includes a surface plant thermal to mechanical energy conversion factor, pump work, and an energy drilling capital cost. To complement the optimization results, detailed parametric studies are also performed. The numerical model is built using the Sandia National Laboratories (SNL) massively parallel Sierra computational framework, while the optimization and parametric studies are driven using the SNL Dakota software package. Together, the optimization and parametric studies presented in this paper will help assess the impact of CLGS parameters (e.g., flow rate, tubing length and diameter, insulation length, etc.) on CLGS performance and optimal energy recovery.

## 1. Introduction

According to the GeoVision 2019 report, as of 2016, the net summer geothermally generated capacity in the U.S. was 2542 MWe (electric) which accounts for 0.4 % of the total U.S. electrical power output, with two states, California and Nevada, accounting for most of this production (U.S. Department of Energy, 2019). Historically, U.S. annual geothermal production has remained between 10,000 – 15,000 GWhe since the late 1980s and only more recently have production levels

returned to the 15,000 GWhe peak (U.S. Department of Energy, 2019). At such a low percentage of total U.S. electrical power output, it is clear that there is room for technical improvements in geothermal systems to better exploit the vast subsurface thermal resources.

Currently, nearly all of the geothermal power production comes from conventional hydrothermal plants located in the western U.S., which operate by extracting heat from naturally occurring hydrothermal reservoirs. The largest of such systems is the 800 MWe Geysers hydrothermal steam field in California, which at its 1987 peak provided roughly 1600 MWe through several hundred production wells (Sanyal, 2016). A significant disadvantage of these systems is the large volumes of water required to replenish the permeable reservoir. For example, to slow the depletion rate of the Geysers field, a 46 km long pipeline was constructed to augment injection by 7.8 million gallons per day using municipal effluent from the Clear Lake community (Sanyal, 2016).

High-grade hydrothermal fields such as the Geyser field are also the exception and not the norm. To increase potential candidate sites, Enhanced Geothermal Systems (EGS) have been proposed. In EGS, low permeability hot-dry-rock zones are hydraulically fractured to increase the permeability to artificially create a geothermal reservoir (Rybach, 2010; Tester et al., 2006). Besides the increased capital expenditures, these systems suffer from lost circulation, exhibit mineral scaling, and have increased uncertainty associated with hydraulic fracturing (van Oort et al., 2021).

Alternatively, in a Closed-Loop Geothermal System (CLGS), the working fluid is entirely enclosed and re-circulated in deeply placed tubing. Unlike conventional hydrothermal systems, CLGS can target hot-wet-rock as well as the more commonly available hot-dry-rock subsurface reservoirs; the latter has been estimated to account for more than 95% of the available geothermal energy (Mock et al., 1997). The two main CLGS designs are the U-tube heat exchanger and the Downhole Coaxial Heat Exchanger (DCHE). Several experimental and numerical studies of these designs have been performed and general design guidelines have been proposed (Amaya et al., 2020; Horne, 1980; Morita et al., 1992; Nalla et al., 2005; Oldenburg et al., 2019; X. Song et al., 2018; X. Z. Song et al., 2018; Sun et al., 2018).

In this study, we consider a U-tube configuration of a CLGS sited in a hot dry rock formation largely representative of the Frontier Observatory for Research in Geothermal Energy (FORGE) site located near Milford, Utah (Moore et al., 2019). The objective of this work is to numerically determine optimal configuration and operating conditions for maximizing mechanical power output for producing electricity. We define an objective function that considers a plant efficiency meant to account for converting thermal to mechanical energy for electricity production. The objective function is penalized by pump work as well as estimated capital costs to emplace the subsurface U-tube. To determine the optimal configuration, a gradient-based optimization search is used.

## 2. Methodology

### *2.1. Governing equations*

Figure 1 shows a schematic of the subsurface portion a CLGS, with a U-shaped borehole circulating a working fluid to extract heat from the formation. The governing equations for the working fluid are simplified to an area-averaged 1D model. The continuity equation assumes a

constant mass flow rate, while the thermal energy equation is simplified to a one-dimensional, area averaged formulation by assuming the fluid temperature $T_{\mathrm{f}}$ and fluid properties are constant through a borehole cross section,

$$\int \rho_{\mathrm{f}} c_{\mathrm{p,f}} \frac{\partial T_{\mathrm{f}}}{\partial t} + \rho_{\mathrm{f}} c_{\mathrm{p,f}} u_{\mathrm{f}} \frac{\partial T_{\mathrm{f}}}{\partial z} \mathrm{d}\Omega = -\int q \cdot \hat{\mathrm{n}}\, d\Gamma \tag{1}$$

where $\rho_{\mathrm{f}}$, $c_{\mathrm{p,f}}$, and $u_{\mathrm{f}}$ are the density, specific heat, and velocity of the water. Here, the volume integral is over the borehole volume, whereas the surface integral is over the circumferential borehole area. The axial diffusive flux was ignored as it is negligible compared to the advective flux for the problems considered here. The viscous dissipation term, as well as the heating and or cooling of the fluid material due to pressure variations (i.e., water has a small bulk expansion coefficient), were also ignored. The surface integral of the heat flux couples the working fluid to the formation and is defined as,

$$-q \cdot \hat{n} = -\mathrm{U}(\mathrm{T_f} - T_{\mathrm{s,i}}) \tag{2}$$

where $T_{\mathrm{s,i}}$ is the temperature of the solid formation at the interface. Here, the effective heat transfer coefficient $U$ includes an in-series wall thermal resistance $R_{\mathrm{ins}}$ modeling a thin layer of insulation

$$U = \frac{1}{\frac{1}{h_{\mathrm{f}}} + R_{\mathrm{ins}}} \tag{3}$$

where $h_{\mathrm{f}}$ is the heat transfer coefficient for the working fluid defined as,

$$h_{\mathrm{f}} = \frac{k_{\mathrm{f}}}{D} Nu \tag{4}$$

where $D$ is the hydraulic diameter of the cross section and $Nu$ is the Nusselt number. For turbulent flows in pipes, the Gnielinski correlation is used to calculate the Nusselt number (Incropera & Incropera, 2007)

$$Nu = \frac{\frac{f}{8}(Re_{\mathrm{D}} - 1000)Pr}{1.0 + 12.7\left(\frac{f}{8}\right)^{1/2}(Pr^{2/3} - 1)} \tag{5}$$

where $f$ is the smooth tube friction factor, $Pr = \frac{\nu_{\mathrm{f}}}{\alpha_{\mathrm{f}}}$ is the working fluid's Prandlt number with $\nu_{\mathrm{f}}$ the kinematic viscosity and $\alpha_{\mathrm{f}}$ the thermal diffusivity, and $Re_D$ is the Reynolds number,

$$Re_{\mathrm{D}} = \frac{4\dot{m}}{\pi D \mu_{\mathrm{f}}} \tag{6}$$

where $\dot{m}$ is the constant mass flow rate, and $\mu_{\mathrm{f}}$ is the dynamic viscosity.

For fluid momentum conservation, a steady force balance is considered between fluid pressure $P_{\mathrm{f}}$ shear, and gravitational forces,

$$\int \frac{\partial P_{\mathrm{f}}}{\partial z} d\Omega = \int F_{\mathrm{b}} d\Omega - \int \tau_{\mathrm{w}}\, d\Gamma \tag{7}$$

Here, $\tau_w$ is the wall shear stress modeled using the Darcy-Weisbach friction factor formulation (Incropera & Incropera, 2007),

$$\tau_w = \frac{1}{8} f \rho_f u_f^2 \tag{8}$$

where the non-dimensional wall shear stress i.e., the friction factor, is obtained through the explicit Haaland fitting (Munson et al., 2013),

$$\frac{1}{\sqrt{f}} = -1.8 \log\left[\left(\frac{\epsilon/D}{3.7}\right)^{1.11} + \frac{6.9}{Re}\right] \tag{9}$$

The outlet pressure was held fixed such that the water remained in the liquid phase. For most of the design space, an outlet pressure of 1.6 MPa was used to keep water in a liquid phase, though in some instances higher outlet pressures of up to 3 MPa were needed. At the expected operational temperature range (25 – 225 $^{o}$C), the material properties of water do not vary significantly with pressure and can be treated as strictly functions of the temperature, thereby decoupling the 1D momentum equation from the 1D thermal energy equation, i.e., the pressure can be explicitly integrated along the path. The temperature dependent material properties of water are tabulated at a constant reference pressure $P_{ref} = 15$ MPa using CoolProps (Bell et al., 2014) with the exception of the enthalpy which is evaluated retrospectively using updated estimates of pressure in the system.

For the hot dry rock, the conservation of thermal energy statement is,

$$\int \rho_s c_{p,s} \frac{\partial T_s}{\partial t} d\Omega = \int \nabla \cdot k_s \nabla T_s d\Omega \tag{10}$$

where $T_s$ is the formation temperature, $\rho_s$, $c_{p,s}$, and $k_s$ are the bulk density, specific heat, and thermal conductivity of the rock formation, respectively. The rock formation is coupled to the working fluid through an equal and opposite heat flux prescribed at the working fluid – formation interface.

The system of equations is solved using the Sandia National Labs (SNL) Sierra finite element framework (Sierra Thermal Fluids Development Team, 2021), where the weak formulation of the coupled partial differential equations is discretized over the domain using linear (working-fluid) and bilinear elements (formation) with SUPG stabilization applied to the advective term. The resulting discrete non-linear system of equations are solved using Newton iterations with preconditioned GMRES iterations applied to the inner linear system.

### *2.2. Optimization*

In the U.S., geothermal systems have a total power generation capacity of approximately 3800 MWe. In contrast, the low-temperature geothermal applications total approximately 100 MWth. It is clear that, in the U.S., the predominant use for geothermal systems is to generate electricity (2019). As such, this paper focuses on optimizing a mechanical objective function, defined as (White et al., 2021),

$$F_{\text{mech}} = \int_0^T \left( \dot{m} \Delta h_{\text{f}} \eta - \frac{1}{\eta_{\text{p}}} \max\left(\dot{W}_{\text{p}}, 0\right) \right) dt - \frac{CL}{C_{\text{e}}} \tag{11}$$

Here, the integral of the first term represents the mechanical energy that can be extracted from the system over an operational time period $T$ where $\dot{m}$ is the mass flow rate, $\Delta h_{\text{f}}$ is the change in water enthalpy between the outlet and inlet, and $\eta$ is the plant efficiency for converting thermal to mechanical energy. The plant efficiency is approximated as a percentage of the theoretical limit set by the Carnot efficiency, i.e. $\eta = 0.678\eta_{carnot}$, where the Carnot efficiency is determined by the hot and cold temperatures of the system. This percentage was estimated using a linear fitting of geothermal plant efficiencies for varying reservoir temperatures (Zarrouk & Moon, 2014). While this is a rough approximation, it is in good agreement with a more detailed binary plant analysis detailed by the working group (White et al., 2021).

The integral of the second term represents the required pump work over the operational period with $\eta_{\text{p}}$ the pump efficiency and $\dot{W}_{\text{p}}$ the pumping power required

$$\dot{W}_{\text{p}} = \dot{m}\left(\frac{P_{\text{in}}}{\rho_{\text{in}}} - \frac{P_{\text{out}}}{\rho_{\text{out}}}\right) \tag{12}$$

Here, a constant pump efficiency of $\eta_{\text{p}} = 0.65$ is assumed. Note when the outlet pressure, $P_{\text{out}}$, is greater than the inlet pressure, $P_{\text{in}}$, a thermosiphon is possible, and so the required pump work is zero.

In addition to the pump work, the remaining energy penalty term represents how much of the generated electrical power needs to be sold by the plant to recover drilling capital costs. Here, $L$ is the total drilling length in meters, $C$ is the drilling cost in dollars per meter, and $C_{\text{e}}$ is the price at which electricity can be sold. Throughout this work, a base-line drilling cost of $C = 1640$ \$/m is used. Furthermore, for simplicity, the price of electricity has been assumed fixed at \$104,500 per GWhe.

The above scalar objective function is a multi-variable function depending on a number of model parameters (e.g., mass flow rate, CLGS design params, formation gradient and thermal properties, and working fluid properties). To maximize this function, some parameters are chosen as design variables and are bounded to appropriate intervals while others are simply fixed. This optimization problem is formulated and driven using the SNL Dakota package (Dalbey et al., 2020). To solve the optimization problem, the Fletcher-Reeves conjugate gradient method is applied with central differences used to determine numerical gradients during the search procedure.

## 3. Results

### *3.1. U-tube Heat Exchanger*

As shown in Figure 1, in a "U-tube" heat exchanger design, a single U-shaped borehole is drilled into the reservoir. This design consists of a descending vertical borehole ($L_1$), a horizontal borehole ($L_2$), and an ascending vertical borehole ($L_3$), with a smooth transition (not shown) between vertical and horizontal boreholes maintained by varying the drilling angle.

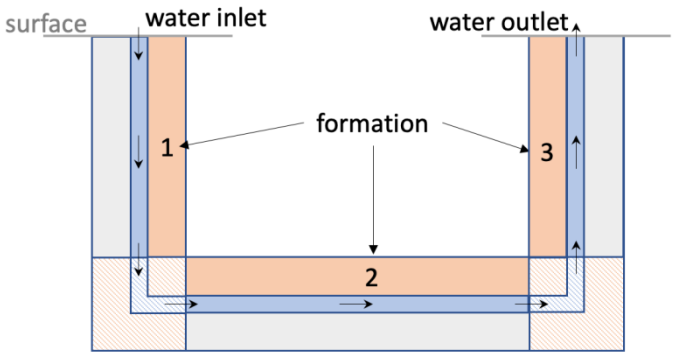


**Figure 1: "U-tube" heat exchanger design. Cold water is injected at the inlet and re-surfaces heated at the outlet.**

Figure 2 shows the computational model used to approximate the above closed loop U-tube design. Here, the following modeling assumptions have been made: 1) the reservoir is hot dry rock so heat transfer to the working fluid is through heat conduction, 2) the thermal resistance of the pipe and casing are ignored except for a thin layer of insulating material in the ascending section which is modeled using an in series thermal resistance added to the fluid heat transfer coefficient 3) the formation heat conduction at the interface between region 1-2 and region 2-3 is negligible, 4) a 2D axisymmetric assumption is valid in each region, 5) the horizontal formation has a constant initial temperature corresponding to the temperature at the max borehole depth, and 6) the "elbow" sections of the U-tube (see Figure 1) can be ignored as the difference in surface area in contact with the formation is negligible compared to the rest of the U-tube. Assumptions 4 and 5 were verified using a 3D model of the formation, showing a negligible impact of the geothermal gradient on the horizontal leg. Adiabatic boundary conditions are applied to the remaining formation boundaries and the formation outer radius is set to 150 m, which was sufficient to enclose the thermal drawdown from energy extraction at the borehole.

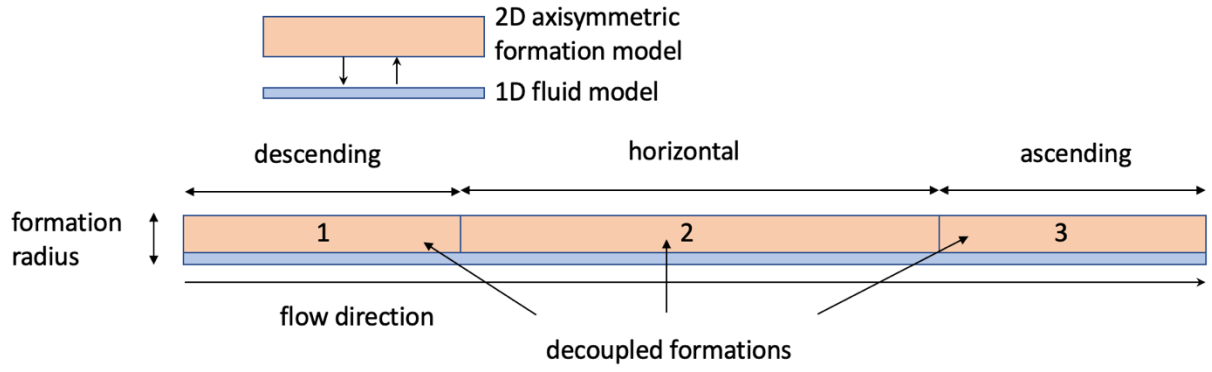


**Figure 2: 2D axisymmetric model for the U-tube closed loop geothermal systems. The mesh (not shown) is biased towards the borehole to resolve the radial temperature gradients. While the formations are assumed to not directly interact, all three formations are still coupled to each other through the heat exchange with the 1D fluid model.**

### 3.1.1 Validation and Verification

Song et al. performed a numerical study of a U-tube design for the Xinji thermal reservoir located in Hebei, China (X. Z. Song et al., 2018). The configuration validated here is as follows. Cold water is injected at 30 ℃ at varying flow rates through a 0.07148 m radius pipe that descends 3.5 km to a 6 km horizontal section. The heated liquid water then resurfaces through a 3.5 km production well bore. The reported Xinji thermal reservoir characteristics used in the simulation are summarized in Table 1.

Figure 3 compares the outlet temperature of the model over a 20-year operational period to Song et al. as well as to the Stanford group's analytic solution (Horne & Shinohara, 1979). As shown, our model nearly overlaps the Stanford analytic solution and slightly underpredicts the numerical results reported by Song et al.

*Table 1. Formation thermal characteristics for the Xinji thermal reservoir.*

| Bulk density [kg/m3] | Specific heat capacity [J/kg-K] | Thermal conductivity [W/m-K] | Surface temperature [℃] | Formation gradient [℃/km] | Bottom borehole temperature [℃] |
|---|---|---|---|---|---|
| 2200 | 850 | 3.0 | 25 | 30 | 130 |

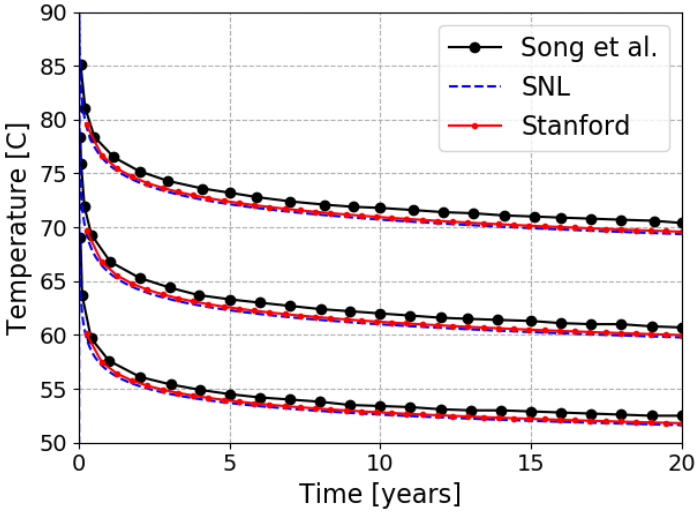


**Figure 3: Outlet temperature for a U-tube sited in the Xinji thermal reservoir compared to Song et al. as well as to the Stanford analytic solution for varying flow rates of $Q$ = 40, 60, and 90 m³/hr. Higher outlet temperatures correspond to decreasing flow rates.**

Song et al. include a conductive cement casing along the horizontal leg as well as an insulating cement casing along the ascending section, whereas the model used here neglects these additional details in order to directly compare against the Stanford analytic solution. Consequently, the slight underprediction of the outlet temperature is expected. The small difference in outlet temperature suggests the specific casing and insulation configuration used in their model has a small impact on the performance of the system. More importantly, the excellent agreement with the Stanford analytic solution indicates that for this specific problem the heat transfer coefficient may

effectively be treated as infinite (Carslaw & Jaeger, 1959). That is, any sufficiently large heat transfer coefficient value will produce approximately the same solution.

### 3.1.2 FORGE site

Using the U-tube model, optimization and parametric studies are carried out to find an optimal configuration that maximizes the net electrical power output for the geological setting at the Frontier Observatory for Research in Geothermal Energy (FORGE) site located near Milford, Utah (Moore et al., 2019).

Compared to the average world geothermal gradient of 30 ℃/km (van Oort et al., 2021) the FORGE site is reported to have increased geothermal gradients ranging from 60-90 ℃/km (Allis et al., 2019). Table 2 summarizes additional relevant thermal characteristics used here for the FORGE site. To reach the target bottom borehole temperature of 225 ℃, a vertical borehole depth of just over 2.5 km is needed with the higher-than-average formation gradient of 78.8 ℃/km used here.

*Table 2. Formation thermal characteristics for the FORGE site.*

| Bulk density [kg/m3] | Specific heat capacity [J/kg-K] | Thermal conductivity [W/m-K] | Surface temperature [℃] | Formation gradient [℃/km] | Bottom borehole temperature [℃] |
|---|---|---|---|---|---|
| 2750 | 790 | 3.05 | 25 | 78.8 | 225 |

Besides the fixed formation properties, additional fixed parameters include the operational period of forty years, the cold-water injection temperature of 300 K, and a pipe surface roughness equal to 0.025 mm. Additionally, as a diameter penalty term was not considered in the objective function, the diameter was chosen to be fixed to D = 0.2159 m (8.5”) for the subsequent discussion. Increases to the pipe diameter have a modest impact on power output through increased heat transfer surface area and reduction of pumping power requirements (assuming the U-tube does not operate as a thermosiphon).

The chosen design parameters for optimization are the mass flow rate, the U-tube’s horizontal length, and the length of insulation at the ascending wellbore as measured from the production outlet. These design parameters are restricted to the following bounds: [1,60] kg/s, [1,10] km for the horizontal length, and [0, 2.5] km for the insulation length. For the portion of the pipe wall that is insulated, a constant thermal resistance of $R_{ins} = 0.383$ m$^2$-K/W is added in series to the fluid heat transfer coefficient. This resistance corresponds to a 0.01 m thick insulating material with a low thermal conductivity of 0.025 W/K-m.

As highlighted in Table 3, using an initial guess of 20 kg/s, 2 km of horizontal length, and 1 km of insulation length, the gradient-based search converges to 10.8 kg/s, 10 km, and 1.4 km, respectively. These design variables correspond to a peak objective value of $F_{\text{mech}}$ = 88 GWhe and a peak mechanical energy output of 324.6 GWhe. The positive objective function indicates the capital drilling costs will be re-couped over the forty years. If instead a shorter operational period of 20 years is specified, capital drilling costs will not be re-couped. The mechanical energy

output indicates the optimal U-tube design can power 765 homes over the specified operational period, assuming an average U.S. home power usage of 10.6 MWhe per year (2019).

*Table 3. Optimal design parameters and the corresponding mechanical objective and mechanical energy output for the FORGE site over a forty-year operational period for a pipe diameter of 0.2159 m.*

| mass flow rate [kg/s] | horizontal length [km] | insulation length [km] | mech. obj. [GWhe] | mech. energy output [GWhe] |
|---|---|---|---|---|
| 10.8 | 10 | 1.4 | 88 | 324.6 |

We note the necessary condition of a zero objective function gradient was not satisfied, i.e., the chosen design is not a true optimum. Further increasing the horizontal length will still result in a net positive impact on the objective function through increased residency times as well as increased surface area, both of which increase the heat transferred to the water. Eventually, we expect an optimum to be reached as the working fluid approaches the bottom borehole temperature; however, this optimum does not lie within our specified 10 km upper-bound for the horizontal leg.

**Error! Reference source not found.** compares the formation borehole surface temperature (solid lines) with the water temperature (dotted lines) at several different time snapshots for the optimal design parameters. Following the path of the injected water, we see that the majority of the temperature rise occurs at maximum depth (i.e., peak temperatures) as the water passes through the horizontal leg ($L_2$) and draws heat from the surrounding hot-dry-rock. Over time, thermal drawdown of the formation reduces the heat flux received by the water and leads to a reduction in the temperature rise.

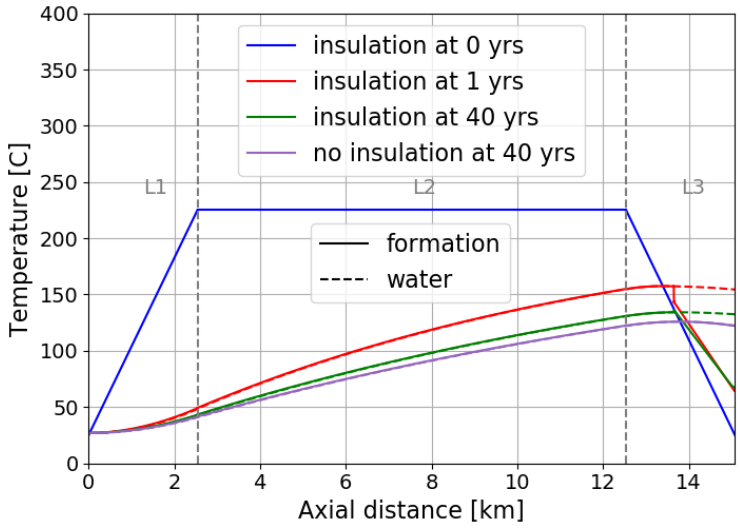


**Figure 4: Comparison of the formation surface temperature (solid line) and water temperature (dotted line) along the axial distance for the optimal parameters listed in Table 3.**

As the hot water passes through the ascending section ($L_3$), it eventually enters the insulated section where a reduced heat transfer coefficient enhances heat recovery. As shown in **Error! Reference source not found.**, this optimal insulation length corresponds to approximately 1.4 km below the surface and results in an abrupt temperature difference between the formation surface and water.

This insulation length corresponds to the average length over which the ascending pipe should be insulated for the given operational period in order to minimize heat loss to the surrounding formation. The temperature cross-over point i.e., where the ascending hot water's temperature exceeds the formation surface's temperature, is not shown and in general will vary with time and position in $L_3$. **Error! Reference source not found.** also highlights that not using insulation results in a modest reduction in temperatures. Moreover, without insulation, both temperature profiles appear nearly coincident, indicating the heat transfer coefficient is effectively infinite.

Figure 5 shows the water outlet temperature as a function of time with and without insulation. Without insulation added to the ascending section, a decrease of approximately 10 ℃ is observed in the outlet temperature. Additionally, due to the thermal drawdown of the surrounding hot-dry-rock (see Figure 6), a decrease from a year-one outlet temperature of 154.5 ℃ to an end-of-life outlet temperature of 132.5 ℃ is observed for the case with insulation.

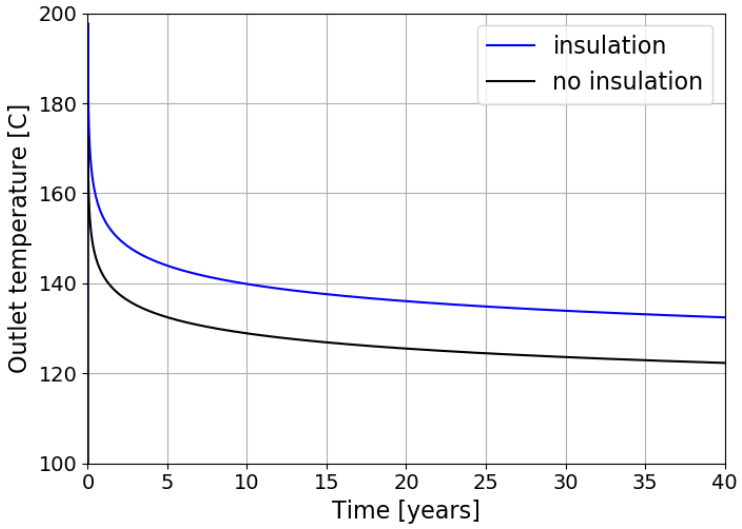


**Figure 5: Water outlet temperature as a function of time for the FORGE site optimal design parameters listed in Table 3 with a pipe diameter of $D$ = 0.2159 m with and without insulation.**

Throughout the operational period, the optimal design averages a mechanical power output of 926 kWe. By the end of the operational period, the power output of the chosen design drops to 848 kWe, whereas the thermal power output at end-of-life is 4.81 MWth. This stark contrast is due to a low end-of-life outlet temperature which corresponds to a plant efficiency of approximately $\eta = 0.18$.

Figure 6 highlights the extent of the radial penetration at 1, 5, 20, and 40 years at the midpoint of the three U-tube sections. As can be seen, the majority of the thermal depletion occurs within a radius of 100 m near the borehole. The accompanying decrease in the formation temperature results in an overall reduced heat flux to the working fluid and correspondingly, a gradual drop in the outlet temperature. The temperature at the midpoint of the ascending section ($L_3$) remains almost constant due to the insulation added to the pipe.

To better understand the design space, two dimensional parametric studies were performed. The design space was sampled using a 21x21 uniformly spaced grid in two specified planes. In Figure 7, contours for the objective function, mechanical energy output, pump work and average Carnot

efficiency are shown in the mass flow rate vs. horizontal length plane for $D$ = 0.2159 m without insulation (i.e., the front view of the three dimensional design space).

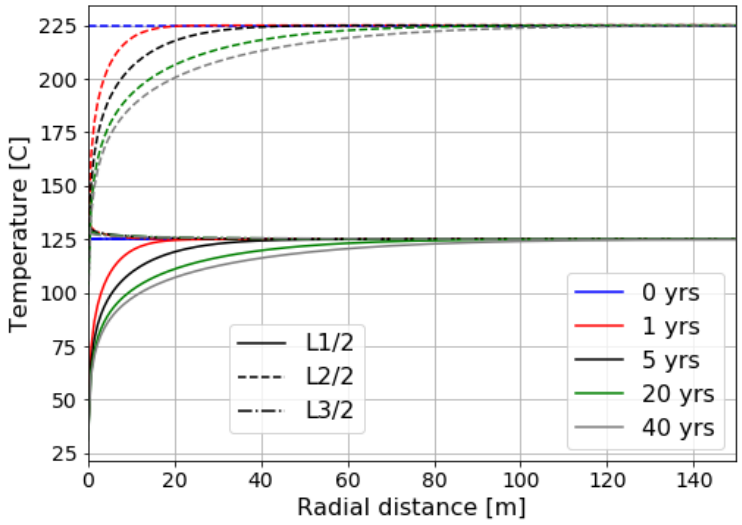


**Figure 6: Temperature as a function of radial distance at 1, 5, 20, and 40 years at the midpoint of the descending (solid), horizontal (dotted), and ascending sections of the U-tube.**

As can be seen from the mechanical objective function contours in Figure 7a, most of the design space is not economically viable at the specified drilling cost (1640 $/m). The resulting feasibility envelope (i.e., the zero-level set) is quite narrow but widens with longer horizontal lengths as higher mass flow rates become accessible due to increased residency times. The feasibility envelope has a strong dependence on the base-line drilling cost. While it is possible to re-compute the contours for a lowered drilling cost or to compute break-even drilling cost contours, it is more instructive to look at the idealized scenario of zero drilling cost and zero pump work i.e., the mechanical energy that can be extracted from the system.

Figure 7b indicates a peak mechanical work output of 307.6 GWhe can be produced without using insulation on the ascending wellbore. Here, the optimal mass flow rate is 12.2 kg/s. A comparison of Figure 7b and Figure 7d, indicates the peak mechanical work output does not correspond to the peak average Carnot efficiency. The average Carnot efficiency peaks around a narrow band spread across lower mass flow rates that are inadequate for energy production. The maximum average Carnot efficiency corresponds to an end-of-life outlet temperature of about 169.7 ℃. This narrow band is formed because low mass flow rates result in significant heat loss to the formation in the ascending wellbore, whereas high mass flow rates lead to decreased residency times and therefore less heat extracted. Consequently, a local optimum is expected for each horizontal length.

As evident in Figure 7c, the U-tube operates as a thermosiphon over a large portion of the design space (including the optimal design). This boundary is delineated by the zero-level set curve. On the other hand, a maximum pump work of -33.8 GWh is required for maximum horizontal length and maximum flow rate. The worst operating point occurs at minimum length and maximum flow rate, where the required pump energy input is 1.08 times the mechanical energy that could be extracted from the system. This is primarily due to the decreased residency times which result in an impractical Carnot efficiency of $\eta_{\text{carnot}} \approx 0.028$.

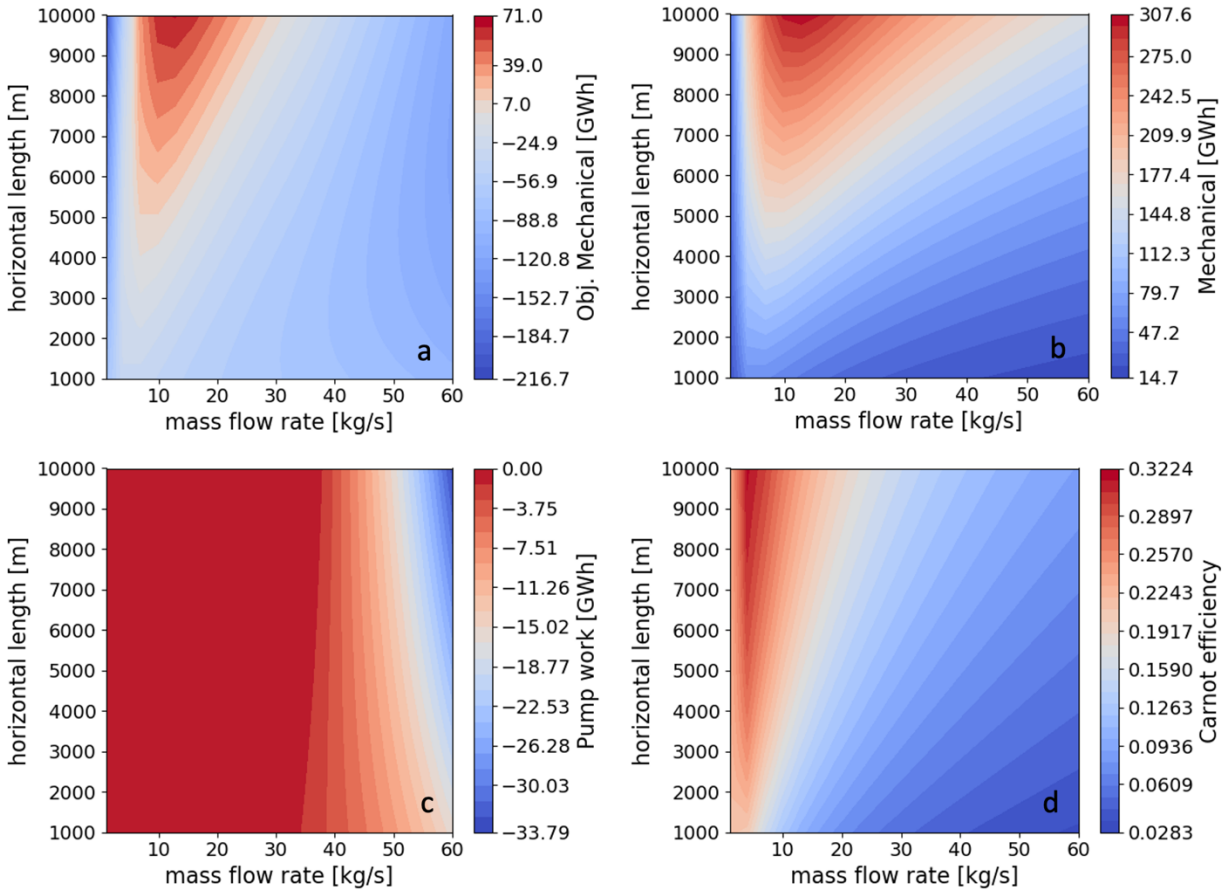


**Figure 7: Objective function (a), mechanical energy (b), pump work (c), and average Carnot efficiency (d) for the FORGE site as a function of horizontal length 1-10 km and mass flow rate 1- 60 kg/s for a fixed diameter of $D = 0.2159$ m without insulation for an operational period of 40 years. The objective function value represents the mechanical (electric) output over 40 years discounted by pumping costs and capital costs of loop emplacement, while the mechanical energy is the unpenalized output.**

In Figure 8, contours for the objective function and mechanical energy output are shown in the mass flow rate vs. insulation length plane for the optimal horizontal length of 10 km (i.e., the top view of the 3D design space). As can be seen by comparing with Figure 7b, insulating the ascending well is only modestly helpful, resulting in about a 5% increase in total mechanical energy output over 40 years.

Not shown is that with insulation, a peak end-of-life outlet temperature of 193.8 ℃ is possible corresponding to an average Carnot efficiency of 0.36. While close to theoretical limit set by the cold and hot (225 $^{o}$C bottom-hole) temperatures of the system, the required low mass flow rate to sustain such high temperatures results in suboptimal mechanical energy production.

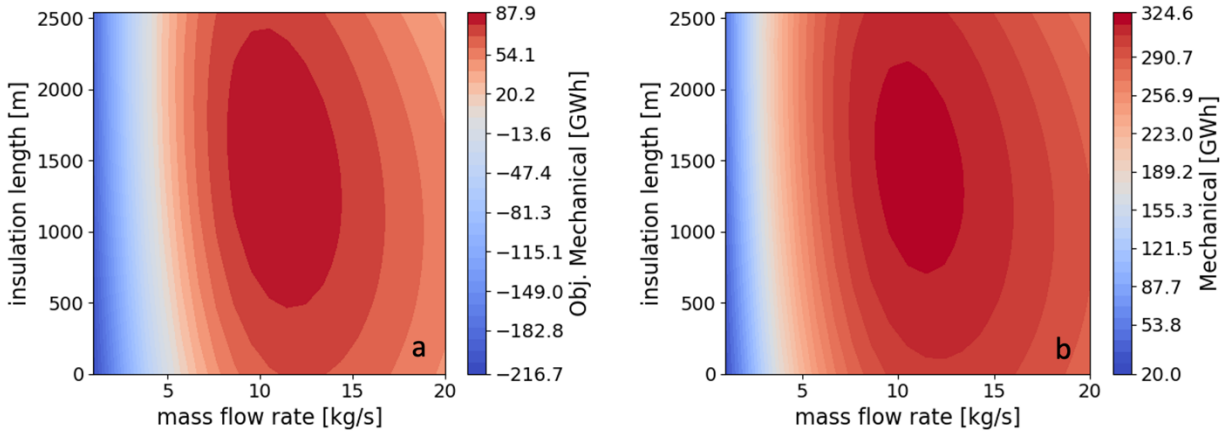


**Figure 8: Mechanical objective (a) and mechanical energy (b) for the FORGE site as a function of insulation length and mass flow rate for a fixed pipe diameter of $D$ = 0.2159 m with horizontal length of 10 km.**

It is useful to briefly quantify the U-tube diameter impact. Ignoring diameter penalties, if the pipe diameter is increased to $D$ = 0.381 m (15”), the gradient-based search will converge to a mass flow rate of 2.26 kg/s, a horizontal length of 10 km, and an insulation length of 1.38 km, close to the same optimal solution, but corresponding to 355.1 GWe of mechanical energy output, or about 1.0 MWe average over the 40-year operational period. Considering the total mechanical output was increased less than 10% yet the required drilling volume to be removed increased by more than 3 times due to the squared dependence on the diameter, it is unclear whether increasing throughput via larger diameters will be economic.

## 4. Summary

Optimization results indicate that an optimal hot-dry-rock CLGS configuration for the FORGE site will result in slightly less than 1 MWe average power output capacity over a forty-year operational period for an 8.5-inch diameter pipe. The following summarizes the highlights of this study:

- Longer horizontal lengths are always better for the considered range of 1-10 km
- The optimal system operates as a thermosiphon (i.e., zero pump work) and is expected to produce 324.6 GWhe over 40 years
- Increasing the U-tube pipe diameter from 0.2159 m (8.5 inch) to 0.381 m (15 inch) increases the mechanical energy output by about 9%.
- For a given length of horizontal leg, there is an optimal flow rate determined by a balance of high Carnot efficiency (high outlet temperature) with enthalpy flux.
- Ascending well insulation helps prevent loss of energy, but the improvement is modest at optimal conditions. Insulation can increase outlet temperature by about 10 $^{o}$C. We did not consider cost of insulation in the study.

**Acknowledgement**

This material was based upon work supported by the U.S. Department of Energy, Office of Energy Efficiency and Renewable Energy (EERE), Office of Technology Development, Geothermal Technologies Office. We would also like to thank the expert panel comprised of Doug Hollett (Melroy-Hollett Technology Partners), Roland Horne (Stanford University), Laura Pauley (Pennsylvania State University), and Chad Augstine (National Renewable Energy Laboratory) as well as other working group members for their guidance and insightful discussions. We would especially like to thank Mark White (Pacific Northwest National Laboratory) for organizing and leading the working group. Sandia National Laboratories is a multimission laboratory managed and operated by National Technology and Engineering Solutions of Sandia, LLC, a wholly owned subsidiary of Honeywell International Inc., for the U.S. Department of Energy's National Nuclear Security Administration under contract DE-NA0003525.

## REFERENCES

Allis, R., Gwynn, M., Hardwick, C., Hurlbut, W., Kirby, S., & Moore, J. N. (2019). Thermal characteristics of the Roosevelt Hot Springs system, with focus on the FORGE EGS site, Milford, Utah. *Utah Geological Survey Miscellaneous Publication 169-D*.

Amaya, A., Scherer, J., Muir, B., Patel, M., & Higgins, B. (2020). GreenFire energy closed-loop geothermal demonstration using supercritical carbon dioxide as working fluid. *45th Workshop on Geothermal Reservoir Engineering*, 10-12.

Bell, I. H., Wronski, J., Quoilin, S., & Lemort, V. (2014). Pure and Pseudo-pure Fluid Thermophysical Property Evaluation and the Open-Source Thermophysical Property Library CoolProp. *Industrial & Engineering Chemistry Research*, *53*(6), 2498-2508. https://doi.org/10.1021/ie4033999

Carslaw, H. S., & Jaeger, J. C. (1959). *Conduction of heat in solids* (2d ed.). Clarendon Press.

Dalbey, K., Eldred, M. S., Geraci, G., Jakeman, J. D., Maupin, K. A., Monschke, J. A., Seidl, D. T., Swiler, L. P., Tran, A., & Menhorn, F. (2020). Dakota A Multilevel Parallel Object-Oriented Framework for Design Optimization Parameter Estimation Uncertainty Quantification and Sensitivity Analysis: Version 6.12 Theory Manual. *SAND2020-4987, Sandia National Laboratory*.

Energy Information Administration. (2019). *Electric Sales, Revenue, and Average Price*. Retrieved from https://www.eia.gov/electricity/sales_revenue_price/

Horne, R. (1980). Design considerations of a down-hole coaxial geothermal heat exchanger. *Geothermal Resources Council Transactions*, *4*(CONF-800920-).

Horne, R., & Shinohara, K. (1979). Wellbore heat loss in production and injection wells. *Journal of Petroleum Technology*, *31*(01), 116-118.

Incropera, F. P., & Incropera, F. P. (2007). *Fundamentals of heat and mass transfer* (6th ed.). John Wiley.

Mock, J. E., Tester, J. W., & Wright, P. M. (1997). Geothermal energy from the earth: its potential impact as an environmentally sustainable resource. *Annual Review of Energy and the Environment*, *22*(1), 305-356. https://doi.org/10.1146/annurev.energy.22.1.305

Moore, J., McLennan, J., Allis, R., Pankow, K., & Rickard, W. (2019). The Utah Frontier Observatory for Research in Geothermal Energy (FORGE): An International Laboratory

for Enhanced Geothermal System Technology Development. 44th Workshop on Geothermal Reservoir Engineering, Stanford, California.

Morita, K., Bollmeier, W. S., & Mizogami, H. (1992). An Experiment to Prove the Concept of the Downhole Coaxial Heat-Exchanger (Dche) in Hawaii. *20th Anniversary - Geothermal Resources Council*, *16*, 9-16.

Munson, B. R., Okiishi, T. H., Huebsch, W. W., & Rothmayer, A. P. (2013). *Fundamentals of fluid mechanics* (7th edition. ed.). John Wiley & Sons, Inc.

Nalla, G., Shook, G. M., Mines, G. L., & Bloomfield, K. K. (2005). Parametric sensitivity study of operating and design variables in wellbore heat exchangers. *Geothermics*, *34*(3), 330-346. https://doi.org/10.1016/j.geothermics.2005.02.001

Oldenburg, C., Pan, L., Muir, M., Eastman, A., & Higgins, B. S. (2019). Numerical simulation of critical factors controlling heat extraction from geothermal systems using a closed-loop heat exchange method. *41st Workshop on Geothermal Reservoir Engineering*.

Parisi, C., Balestra, P., & Marshall, T. D. (2021). Geothermal Analysis modeling and simulation using Idaho National Laboratory' RELAP5-3D-PRONGHORN coupled codes. *Geothermal Resources Council Transactions*, *45*.

Rybach, L. (2010). The future of geothermal energy and its challenges. *Proceedings world geothermal congress*, *29*.

Sanyal, S. K. (2016). Fifty-five years of commercial power generation at The Geysers geothermal field, California: the lessons learned. *Geothermal Power Generation*, 591-608. https://doi.org/10.1016/B978-0-08-100337-4.00020-6

Sierra Thermal Fluids Development Team. (2021). *SIERRA Multimechanics Module: Aria User Manual - Version 5.0* (SAND2021-3921). https://www.osti.gov/biblio/1777075

Song, X., Zheng, R., Li, G., Shi, Y., Wang, G., & Li, J. (2018). Heat extraction performance of a downhole coaxial heat exchanger geothermal system by considering fluid flow in the reservoir. *Geothermics*, *76*, 190-200. https://doi.org/10.1016/j.geothermics.2018.07.012

Song, X. Z., Shi, Y., Li, G. S., Shen, Z. H., Hu, X. D., Lyu, Z. H., Zheng, R., & Wang, G. S. (2018). Numerical analysis of the heat production performance of a closed loop geothermal system. *Renewable Energy*, *120*, 365-378. https://doi.org/10.1016/j.renene.2017.12.065

Sun, F., Yao, Y., Li, G., & Li, X. (2018). Geothermal energy development by circulating CO2 in a U-shaped closed loop geothermal system. *Energy Conversion and Management*, *174*, 971-982. https://doi.org/10.1016/j.enconman.2018.08.094

Tester, J. W., Anderson, B. J., Batchelor, A. S., & Blackwell, D. D. (2006). *Future of Geothermal Energy, Impact of Enhanced Geothermal Systems (EGS) on the United States in the 21st Century* (INL/EXT-06-11746).

U.S. Department of Energy. (2019). *GeoVision, Harnessing the Heat Beneath our Feet*. Retrieved from http://www.osti.gov/scitech

van Oort, E., Chen, D., Ashok, P., & Fallah, A. (2021). Constructing Deep Closed-Loop Geothermal Wells for Globally Scalable Energy Production by Leveraging Oil and Gas ERD and HPHT Well Construction Expertise. *SPE/IADC International Drilling Conference and Exhibition*.

White, M., Martinez, M., Vasyliv, Y., Bran-Anleu A., G., Parisi, C., Balestra, P., Horne, R., Augustine, C., Pauley, L., Hollett, D., Bettin, G., Marshall, T., & Group, C. L. G. W. (2021). Thermal and Mechanical Energy Performance Analysis of Closed-loop Systems in Hot-Dry-Rock and Hot-Wet-Rock Reservoirs. *Geothermal Resources Council Transactions*, *45*.

Zarrouk, S. J., & Moon, H. (2014). Efficiency of geothermal power plants: A worldwide review. *Geothermics*, *51*, 142-153. https://doi.org/10.1016/j.geothermics.2013.11.001